

Experiments and Modeling of the Autoignition of Methyl Pentanoate at Low to Intermediate Temperatures and Elevated Pressures in a Rapid Compression Machine

Bryan W. Weber^{a,*}, Justin A. Bunnell^a, Kamal Kumar^b, Chih-Jen Sung^a

^a*Department of Mechanical Engineering, University of Connecticut, Storrs, CT, USA*

^b*Department of Mechanical Engineering, University of Idaho, Moscow, ID, USA*

Abstract

Methyl valerate ($\text{C}_6\text{H}_{12}\text{O}_2$, methyl pentanoate) is a methyl ester and a relevant surrogate component for biodiesel. In this work, we present ignition delays of methyl valerate measured using a rapid compression machine at a range of engine-relevant temperature, pressure, and equivalence ratio conditions. The conditions we have studied include equivalence ratios (ϕ) from 0.25 to 2.0, temperatures between 680 K and 1050 K, and pressures of 15 bar and 30 bar. The ignition delay data demonstrate a negative temperature coefficient region in the temperature range of 720 K–800 K for both $\phi = 2.0$, 15 bar and $\phi = 1.0$, 30 bar, with two-stage ignition apparent over the narrower temperature ranges of 720 K–760 K for 15 bar and 740 K–760 K at 30 bar. In addition, the experimental ignition delay data are compared with simulations using an existing chemical kinetic model from the literature. The simulations with the literature model under-predict the data by factors between 2 and 10 over the entire range of the experimental data. In addition, a new chemical kinetic model is developed using the Reaction Mechanism Generator (RMG) software. The agreement between the experimental data and the RMG model is also not satisfactory. To help determine the possible reasons for the disagreement, a path analysis of both models is completed. It is found that improvements to both the reaction

*Corresponding Author: bryan.weber@uconn.edu

pathways and thermodynamic properties are required. Further directions for future improvement of the methyl valerate model are discussed.

Keywords: chemical kinetics, rapid compression machine, autoignition, methyl ester, methyl valerate, methyl pentanoate

1. Introduction

For transportation applications, biodiesel is an important constituent in improving environmental friendliness of fuels. This is due to its renewability when produced from sustainable agricultural crops and its ability to reduce emissions relative to petroleum-derived fuels [1]. Biodiesel typically consists of long-chain methyl ester molecules, with typical compositions of C_{14} to C_{20} [1]. Recognizing that the large molecular size of the methyl esters within biodiesel fuel makes creating and using detailed chemical kinetic models challenging [2], it is desired to study their combustion chemistry by studying simpler methyl ester molecules.

A recent review paper summarizes the work on methyl esters relevant to biodiesel combustion [3]; the following summary focuses on ignition delay measurements, since these are the focus of this paper. Autoignition of methyl butanoate (MB, $C_5H_{10}O_2$) has been well-studied in both shock tube and rapid compression machine experiments [4–10]. The prevalence of MB data in the literature is largely due to the early identification of MB as a potential surrogate fuel for biodiesel [11]. However, the literature experiments have shown that MB may not be an appropriate surrogate for biodiesel, due to its lack of negative temperature coefficient (NTC) behavior, a requirement for a suitable biodiesel surrogate [3].

Methyl esters larger than MB, such as methyl valerate (MV, $C_6H_{12}O_2$, methyl pentanoate), have also been studied as possible biodiesel surrogates. Hadj-Ali et al. [9] used a rapid compression machine (RCM) to study the autoignition of several methyl esters including MV. Although MV exhibited two-stage ignition in this study, little additional research has been done on its low-

26 temperature chemistry. Korobeinichev et al. [12] studied MV in premixed lam-
 27 inar flames and extended a detailed high temperature chemical kinetic model
 28 to include MV and methyl hexanoate. Dmitriev et al. [13] added MV to n-
 29 heptane/toluene fuel blends to determine the resulting intermediate species in
 30 premixed flames using a flat burner at 1 atm and an equivalence ratio of 1.75.
 31 The addition of MV helped reduce soot forming intermediates including ben-
 32 zene, cyclopentadienyl, acetylene, propargyl, and vinylacetylene [13]. Hayes
 33 and Burgess [14] computationally examined the peroxy radical isomerization
 34 reactions for MV to better understand the low temperature reaction pathways.
 35 Finally, Diévert et al. [15] used diffusion flames in the counterflow configuration
 36 to determine extinction limits for a number of methyl esters, including MV, and
 37 validated a detailed kinetic model with the experimental data.

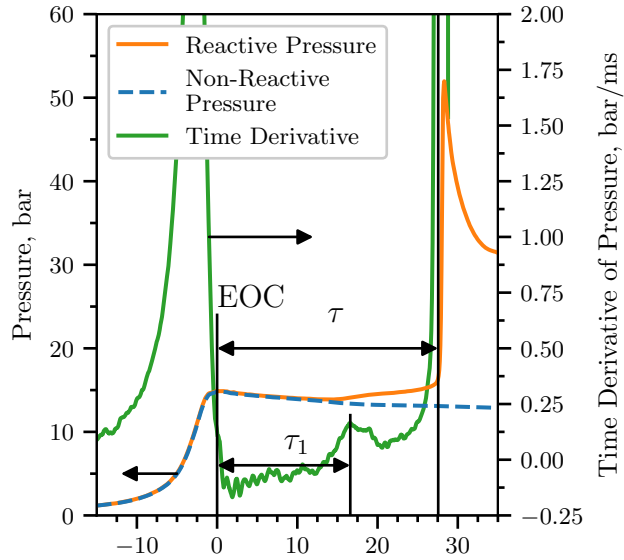
38 This work provides additional data for the autoignition of MV. Data is col-
 39 lected in a RCM under engine relevant conditions spanning from 15 bar to 30 bar,
 40 equivalence ratios (ϕ) from 0.25 to 2.0, and temperatures from 680 K to 1050 K.
 41 The NTC region of MV is mapped out to provide additional information on the
 42 fidelity of using MV as a biodiesel surrogate and insights into the autoignition
 43 chemistry of large methyl esters.

44 **2. Experimental Methods**

45 The RCM used in this study is a single piston arrangement and is pneu-
 46 matically driven and hydraulically stopped. The device has been described in
 47 detail previously [16] and will be described here briefly for reference. The end
 48 of compression (EOC) temperature and pressure (T_C and P_C respectively), are
 49 independently changed by varying the overall compression ratio, initial pressure
 50 (P_0), initial temperature (T_0), and specific heat ratio of the experiments. The
 51 piston in the reaction chamber is machined with a specially designed crevice to
 52 suppress the roll-up vortex effect and promote homogeneous conditions in the
 53 reactor during and after compression [17].

54 The primary diagnostic on the RCM is the in-cylinder pressure measured by

55 a Kistler 6125C dynamic transducer that is compensated for thermal shock. The
 56 transducer is coupled to a Kistler 5010B charge amplifier. The voltage output
 57 of the charge amplifier is recorded by a National Instruments 9125 analog input
 58 device connected to a cDAQ 9178 chassis. The voltage is sampled at a rate of
 59 either 50 kHz or 100 kHz by a LabView VI and processed by a Python package
 60 called UConnRCMPy [18]. Version 3.0.5 of UConnRCMPy [19], 3.6 of Python,
 61 2.3.0 of Cantera [20], 1.13.0 of NumPy [21], 0.19.0 of SciPy [22], and 2.0.1 of
 62 Matplotlib [23] are used in the analysis in this paper.



63

Figure 1: Definition of the ignition delays used in this work. The experiment in this figure
 is conducted for a $\phi = 2.0$ mixture with $\text{Ar}/(\text{N}_2 + \text{Ar}) = 0.5$, $P_0 = 0.7806$ bar, $T_0 = 373$ K,
 $P_C = 14.92$ bar, $T_C = 720$ K, $\tau = (27.56 \pm 0.89)$ ms, and $\tau_1 = (16.60 \pm 0.46)$ ms. The non-
 64 reacting pressure traces by replacing O_2 with N_2 is also shown for reference.

65 The compression stroke of the RCM brings the fuel/oxidizer mixture to the
 66 EOC conditions, and for suitable thermodynamic states, the mixture will ignite
 67 after a delay period. The definitions of the ignition delays are shown in Fig. 1.
 68 The time of the EOC is defined as the maximum of the pressure trace prior to
 69 the start of ignition and the ignition delays are defined as the time from the EOC

until local maxima in the first time derivative of the pressure. Each experimental condition is repeated at least five times to ensure repeatability of the data. As there is some random scatter present in the data, the standard deviation (σ) of the ignition delays from the runs at a given condition is computed. Typically, σ is less than 10 % of the mean values of the overall ignition delay (τ) and the first stage ignition delay (τ_1).

In addition to the reactive experiments, non-reactive experiments are conducted by replacing O_2 with N_2 to determine the influence of machine-specific behavior on the experimental conditions (see Fig. 1) and permit the calculation of the EOC temperature via the isentropic relations between pressure and temperature [24]. The EOC temperature is calculated by the procedure described in Section 3.

The mixtures considered in this study are shown in Table 1. Four equivalence ratios of MV in “air” are considered. While O_2 is kept at 21 % by mole in the oxidizer, the ratio of Ar : N_2 in the oxidizer is varied to adjust the temperatures reached at the EOC. Two P_C conditions are studied in this work, 15 bar and 30 bar, representing engine-relevant conditions. For the $\phi = 2.0$ condition, only $P_C = 15$ bar is considered because we could not achieve T_C values low enough that the ignition during the compression stroke can be prevented.

Table 1: Mixtures considered in this work

ϕ	Mole Fraction (purity)				Ar/($N_2 + Ar$)
	MV (100 %)	O_2 (99.994 %)	Ar (99.999 %)	N_2 (99.999 %)	
0.25	0.0065	0.2087	0.7848	0.0000	1.0
0.5	0.0130	0.2074	0.7796	0.0000	1.0
1.0	0.0256	0.2047	0.7697	0.0000	1.0
1.0	0.0256	0.2047	0.3849	0.3848	0.5
2.0	0.0499	0.1996	0.0000	0.7505	0.0
2.0	0.0499	0.1996	0.3752	0.3753	0.5

Mixtures are prepared in stainless steel mixing tanks, 17 L and 15 L in size. The proportions of reactants in the mixture are determined by specifying the absolute mass of the fuel, the equivalence ratio, and the ratio of Ar : N₂ in the oxidizer. Mixtures are made by first vacuuming the mixing tanks to an ultimate pressure less than 5 Torr. Since MV is a liquid with a relatively small vapor pressure at room temperature and pressure, it is measured gravimetrically to within 0.01 g of the specified value. The fuel is injected into the mixing tank through a septum. Proportions of O₂, Ar, and N₂ are added manometrically at room temperature and the total pressure is measured by an Omega Engineering MMA100V10T2D0T4A6 type static pressure transducer. The same transducer is used to measure the pressure of the reactant mixture prior to an experiment.

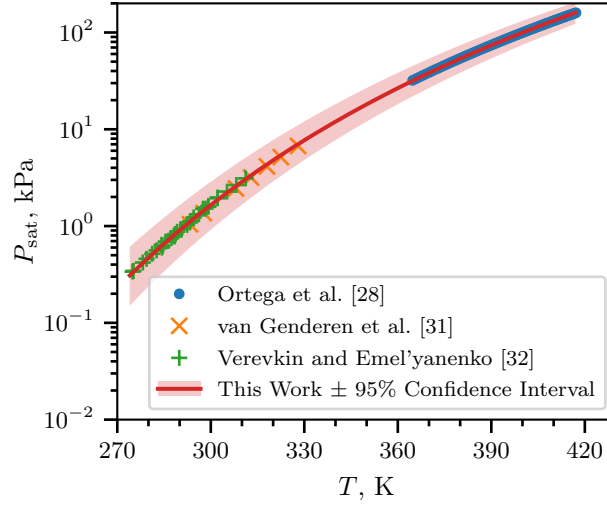
The RCM is equipped with heaters to control the initial temperature of the mixture. After filling in the components to the mixing tanks, the heaters are switched on and the system is allowed 1.5 h to come to steady state. The mixing tanks are also equipped with magnetic stir bars so the reactants are well mixed for the duration of the experiments. Previous work has shown this procedure to completely vaporize the fuel and prevent fuel cracking during the heating process [25–27].

The initial temperature is chosen such that the saturated vapor pressure (P_{sat}) of the fuel at the initial temperature is at least twice the partial pressure of the fuel in the mixing tank. The Antoine equation

$$\log_{10} P_{\text{sat}} = A - \frac{B}{T - C} \quad (1)$$

is used to model the saturated vapor pressure of MV as a function of temperature (T), where A , B , and C are substance-specific coefficients, given in units of K and kPa. Coefficients for Eq. (1) are given in the literature by Ortega et al. [28], Camacho et al. [29], and Stephenson et al. [30]. Unfortunately, the values of the coefficients are different among all three references. Therefore, coefficients for use in Eq. (1) are determined in this work by least squares fitting of the data of Ortega et al. [28], van Genderen et al. [31], and Verevkin and Emel’yanenko [32] using the `curve_fit()` function of SciPy [22] version 0.19.0. Figure 2

119 shows that the coefficients fitted with this procedure give good agreement with
 120 the experimental data; values for the coefficients computed in this work and
 121 reported in the literature works are given in Table 2. The data and code used
 122 to calculate the coefficients are provided in the Supplementary Material.



123

Figure 2: Saturated vapor pressure of MV as a function of temperature, plotted using the
 124 Antoine equation, Eq. (1), with $A = 6.4030$, $B = 1528.69$, and $C = 52.881$.

Table 2: Antoine Equation coefficients computed in this work and obtained from the literature,
 in units of K and kPa. The 2σ confidence interval is estimated by taking the square root of
 125 the diagonals of the covariance matrix returned from `curve_fit()`

	A	B	C	T_{\min} , K	T_{\max} , K
This Work	6.4030	1528.69	52.881	274.9	417.18
2σ Confidence Interval	0.0919	53.47	4.934	—	—
126 Ortega et al. [28]	6.23175	1429.00	62.30	364.75	417.18
Camacho et al. [29]	5.9644	1281.06	75.94	281	547
Stephenson et al. [30]	6.62646	1658.4	42.09	297	411

127 3. Computational Methods

128 3.1. RCM Modeling

129 The Python 3.6 interface of Cantera [20] version 2.3.0 is used for all sim-
130 ulations in this work. Detailed descriptions of the use of Cantera for these
131 simulations can be found in the work of Weber and Sung [18] and Dames
132 et al. [33]; a brief overview is given here. As mentioned in Section 2, non-
133 reactive experiments are conducted to characterize the machine-specific effects
134 on the experimental conditions in the RCM. This pressure trace is combined
135 with the reactive pressure trace and used to compute a volume trace by as-
136 suming that the reactants undergo a reversible, adiabatic, constant composition
137 (i.e., isentropic) compression during the compression stroke and an isentropic
138 expansion after the EOC. The volume trace is applied to a simulation con-
139 ducted in an `IdealGasReactor` in Cantera [20] using the CVODES solver from
140 the SUNDIALS suite [34]. The ignition delays from the simulations are de-
141 fined in the same manner as in the experiments. The time derivative of the
142 pressure in the simulation is computed by second order Lagrange polynomials,
143 as discussed by Chapra and Canale [35]. The volume trace files, the corre-
144 sponding pressure traces, and `volume-trace.yaml` files suitable for use with
145 UConnRCMPy v3.0.5 [19] are available on the web at [https://combdialab.](https://combdialab.engr.uconn.edu/database/rcm-database)
146 [engr.uconn.edu/database/rcm-database](https://combdialab.engr.uconn.edu/database/rcm-database) and on figshare at [https://doi.](https://doi.org/10.6084/m9.figshare.5213341)
147 [org/10.6084/m9.figshare.5213341](https://doi.org/10.6084/m9.figshare.5213341). In addition, ChemKED-format [36] files
148 are available in the main ChemKED database repository at [https://github.](https://github.com/pr-ometh-us/ChemKED-database)
149 [com/pr-ometh-us/ChemKED-database](https://github.com/pr-ometh-us/ChemKED-database).

150 To the best of our knowledge, there are three mechanisms for MV combus-
151 tion available in the literature. The first two, by Korobeinichev et al. [12] and
152 Dmitriev et al. [13], were developed to simulate flames, and do not include the
153 low-temperature chemistry necessary to simulate the conditions in the current
154 RCM experiments. The third model was developed by Diévert et al. [15] and
155 includes low-temperature chemistry of MV, although it was only validated by
156 comparison with flame extinction limits. In converting this mechanism for use in

Cantera, we found that there were many species in the thermodynamic database with multiple data entries. For most of these species the thermodynamic data is identical. However, some species are not exact duplicates. For these species, it is not clear from the thermodynamic database file which data set should be preferred. Since Cantera (and CHEMKIN) choose the first instance of a duplicate species to be used, we retained the first entry for all duplicated species. The detailed model of Diévar et al. [15] includes 1105 species and 7141 reactions, and the Cantera formatted input file is available in the Supplementary Material.

3.2. Reaction Mechanism Generator

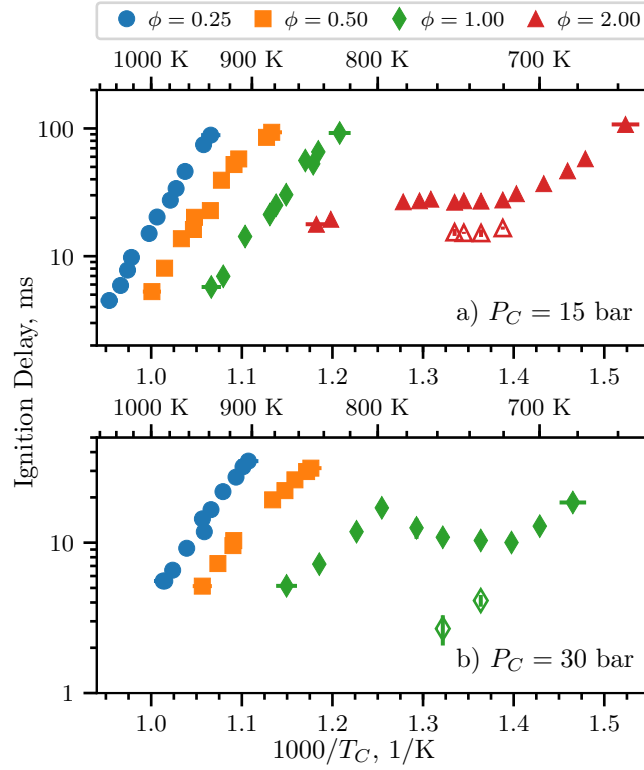
In addition to using a mechanism from the literature, we investigate the use of an automatic mechanism generator, the open-source Reaction Mechanism Generator (RMG) [37] version 2.1.0. The Python version of RMG is used, which requires Python 2.7, and version 2.1.0 of the RMG database is used. The final RMG model contains 427 species and 13640 reactions. Note that the number of species is much lower than the Diévar et al. [15] model because the RMG model focuses on only one fuel (MV), but the number of reactions is substantially higher. The input file used to generate the model is available in the Supplementary Material. In addition, the CHEMKIN and Cantera formatted input files for the RMG-generated model are available in the Supplementary Material.

4. Experimental Results

4.1. Ignition Delays

Figure 3 shows the ignition delay results measured in this study. Filled markers denote the overall ignition delay and hollow markers indicate the first-stage ignition delay. Vertical error bars are drawn on the symbols to represent the 2σ uncertainty in the ignition delay; for many of the experiments, the uncertainty is approximately the same size as the data point, so the error bar is hidden. Horizontal error bars are shown on the first and last points of each equivalence

ratio indicating the estimated uncertainty in the EOC temperature of $\pm 1\%$ [38].
 Fig. 3a shows the results for a compressed pressure of 15 bar, while Fig. 3b shows
 the results for a compressed pressure of 30 bar. Note that $\phi = 2.0$ results were
 not collected for 30 bar, so there are no red triangle data points in Fig. 3b. A
 summary of the ignition delay data is available as a comma-separated value
 file in the Supplementary Material, including the mixture conditions for each
 experiment, the initial conditions, the compressed conditions, and the ignition
 delays and their associated errors.



193

Figure 3: Ignition delays of MV as a function of inverse temperature for varying equivalence ratios. Filled points are the overall ignition delays and hollow points are the first stage ignition delays. a) 15 bar, b) 30 bar.

194

It can be seen from Fig. 3 that the ignition delays for the $\phi = 0.25$ and 0.5 mixtures do not show an NTC region of the ignition delay for both of the pressures studied in this work. However, the $\phi = 1.0$ mixture shows an NTC

197

198 region at $P_C = 30$ bar between approximately 720 K and 800 K, with measured
 199 first-stage ignition delays at 733 K and 757 K. In addition, the $\phi = 2.0$ mixture
 200 shows an NTC region of ignition delay at 15 bar from approximately 720 K to
 201 780 K, with measured first-stage ignition delays between 720 K and 750 K.

202 Hady-Ali et al. [9] also observed two-stage ignition of MV in stoichiometric
 203 mixtures, stating that “[m]ethyl pentanoate... was more reactive [than methyl
 204 butanoate] with a limit below which autoignition no longer occurs observed at
 205 $T_c = 670$ K and $P_c = 11.4$ bar. At this temperature, the autoignition occurred
 206 in two stages with a clearly identified cool flame event.” However, we do not
 207 find two-stage ignition for the similar pressure of $P_C = 15$ bar in this study.
 208 We note that the stated temperature of the experiment from the work of Hady-
 209 Ali et al. [9] (670 K) is much lower than the lowest temperature we considered
 210 in this work at 15 bar, $\phi = 1.0$ (828 K). We did not conduct experiments at
 211 lower temperatures because the work of Mittal and Sung [17] showed that the
 212 temperature field in the RCM reaction chamber was uniform for approximately
 213 100 ms after the EOC, and our measured ignition delay at 15 bar, $\phi = 1.0$, and
 214 828 K is 92.14 ms.

215 However, we find NTC behavior of the overall ignition delay and two-stage
 216 ignition at the higher pressure of 30 bar, and at higher temperatures than those
 217 reported for two-stage ignition in the study of Hady-Ali et al. [9]. The trend
 218 of NTC behavior shifting to higher temperatures with increasing pressure can
 219 be seen in other classes of fuels. Kukkadapu et al. [39] found a similar trend
 220 in gasoline composed of iso-alkanes, n-alkanes, cyclo-alkanes, aromatics, and
 221 olefins. Kukkadapu et al. [39] attributed the shift of the NTC region to the
 222 reactions between the hydroperoxyalkyl radical (QOOH) and O_2 becoming more
 223 dominant than the unimolecular decomposition of QOOH at higher pressures.
 224 Similar trends could occur for the hydroperoxyalkyl radicals of MV.

225 To further understand the effect of the methyl ester functional group on the
 226 NTC region of ignition delay, we compare with the alkane and alcohol with
 227 5-carbon alkyl chains, n-pentane and n-pentanol. n-Pentane and MV have the
 228 same fuel mole percentage for stoichiometric mixtures in air (2.56 %), while

229 n-pentanol has a fuel mole percentage of 2.72 % for stoichiometric conditions.
 230 Ribaucour et al. [40] and Bugler et al. [41] found the NTC region for n-pentane
 231 to be between 760 K and 910 K at pressures near 10 atm. As we will compare
 232 with our MV data at 30 bar, we note that increasing the pressure tends to shift
 233 the NTC to higher temperatures, as mentioned previously [39]. Heufer et al. [42]
 234 found NTC behavior for n-pentanol in the range of 770 K to 900 K at 30 bar. In
 235 this study, we find the NTC window for MV at 30 bar to be between 720 K and
 236 800 K. Therefore, it appears that the methyl ester functional group causes the
 237 NTC range to occur at lower temperature as compared to alkanes and alcohols
 238 with similar alkyl chain lengths. This result was also noted by Hadj-Ali et al.
 239 [9] for methyl hexanoate as the fuel.

240 4.2. Pressure Traces

241 Figure 4a shows the pressure traces for selected experiments at $\phi = 1.0$, $P_C =$
 242 30 bar. The three reactive pressure traces shown are at the low-temperature end
 243 of the NTC (blue, 700 K), one case with two-stage ignition (orange, 733 K), and
 244 one case near the high-temperature limit of the NTC region (green, 774 K). Also
 245 shown is the non-reactive pressure trace for the 700 K case (red). By comparing
 246 the 700 K pressure trace with the non-reactive pressure trace, it can be seen
 247 that there is substantial heat release prior to main ignition as measured by the
 248 deviation of the reactive pressure trace from the non-reactive trace. However,
 249 there is only one peak in the time derivative of the pressure, so no first-stage
 250 ignition delay is defined for this case. It can also be seen in Fig. 4a that the
 251 774 K case shows some heat release prior to ignition, although again there is
 252 only one peak in the time derivative of the pressure. Furthermore, the heat
 253 release at 774 K appears to be more gradual than at 700 K.

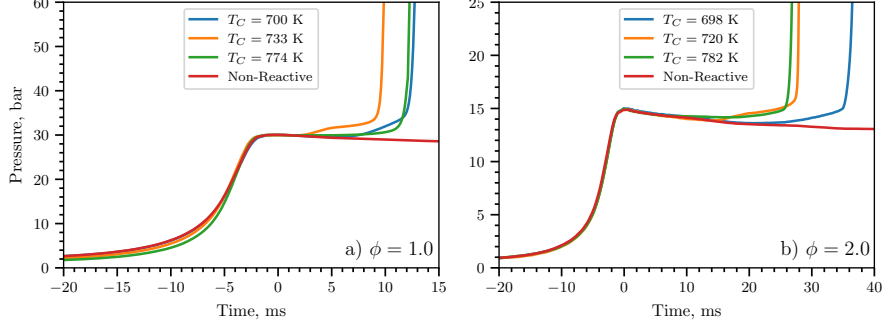


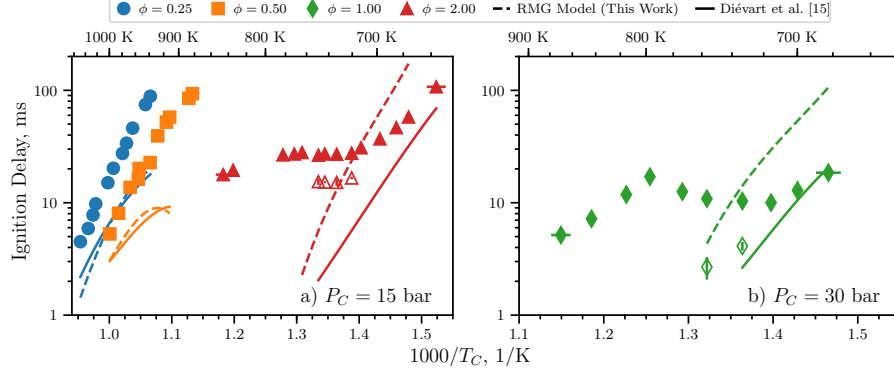
Figure 4: Selected pressure traces around the NTC region of ignition delay. a) $\phi = 1.0$, $P_C = 30$ bar, b) $\phi = 2.0$, $P_C = 15$ bar. The corresponding non-reactive pressure traces are also included for reference.

A similar trend can be observed in Fig. 4b for $\phi = 2.0$ at $P_C = 15$ bar, where pressure traces at several points around the NTC region are plotted. As in Fig. 4a, the three reactive pressure traces shown are at the low-temperature end of the NTC (blue, 698 K), one case with two-stage ignition (orange, 720 K), and one case near the high-temperature limit of the NTC region (green, 782 K). Also shown is the non-reactive pressure trace for the 698 K case (red). As for the $\phi = 1.0$ case, the pressure traces show significant heat release prior to the overall ignition, as judged by deviation from the non-reactive case.

5. Computational Results

Figure 5 compares experimentally measured overall ignition delays with ignition delays computed with the detailed model of Diévar et al. [15] (solid lines). Figure 5a shows results at $P_C = 15$ bar, while Fig. 5b shows results at $P_C = 30$ bar. Only some equivalence ratios are shown for each pressure condition; data and simulated results are not shown for cases where the reactive simulated temperature at the EOC deviated substantially from the non-reactive temperature due to heat release during the compression stroke. Furthermore, it is important to note that the model of Diévar et al. [15] was not validated for MV ignition delays, only for extinction strain rates.

274



275

Figure 5: Comparison of experimental (τ and τ_1) and simulated (τ) ignition delays computed using the procedure described in Section 3.1. a) 15 bar, b) 30 bar.

277

278

279

280

281

282

283

284

285

286

287

288

289

290

291

292

At 15 bar, the experimental overall ignition delays are under-predicted by the Diévert et al. [15] model for the three equivalence ratios shown. For the $\phi = 0.25$ and 0.5 conditions, the model appears to be predicting an NTC region of the overall ignition delays as the temperature decreases, as judged by the increasing curvature of the simulations, although such a trend is not observed apparent in the figure. However, at $\phi = 2.0$, the model does not predict the presence of an NTC region, although one is present in the experiments. Nonetheless, the agreement seems to be improving as the temperature is decreased. Comparing the Diévert et al. [15] model to the stoichiometric data at 30 bar, we find a similar trend as the $\phi = 2.0$, $P_C = 15$ bar data. The model does not predict the NTC region found experimentally for the $\phi = 1.0$, $P_C = 30$ bar experiments, but the agreement improves as the temperature decreases. Interestingly, two-stage ignition is predicted for all of the $\phi = 1.0$ and $\phi = 2.0$ data shown in Fig. 5. However, the first-stage ignition delays are 0.1 ms to 0.5 ms less than the overall ignition delays, and are not shown on Fig. 5 because they are nearly indistinguishable from the overall ignition delay.

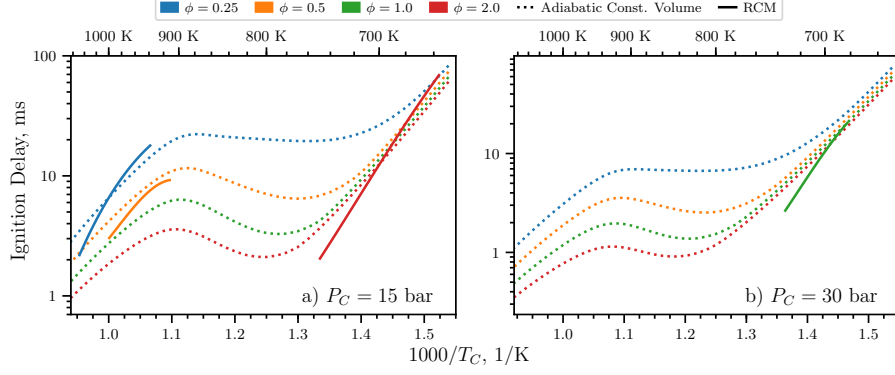


Figure 6: Comparison of simulated ignition delays computed in an adiabatic, constant volume system (dotted lines) and computed using the procedure described in Section 3.1 (solid lines). a) 15 bar, b) 30 bar.

To further understand the model of Diévert et al. [15], we have conducted adiabatic, constant volume simulations (called CONV simulations), as these simulations are not linked to a particular experiment by the volume trace and can be conducted over a wide range of temperatures. In the CONV simulations, overall ignition delay is defined as an increase in the temperature of 400 K over the initial temperature. Figure 6 compares the CONV simulations to the RCM simulations shown in Fig. 5. From Fig. 6, it can be seen that the curvature in the RCM simulations at $P_C = 15$ bar, $\phi = 0.25$ and 0.5 is related to the NTC region of the overall ignition delay, while the lack of curvature in the $P_C = 15$ bar, $\phi = 2.0$ and the $P_C = 30$ bar, $\phi = 1.0$ simulations is because those lie on the low-temperature side of the predicted NTC. It is clear from Fig. 6 that the model of Diévert et al. [15] predicts the NTC to occur at too high a temperature relative to the experiments.

To elucidate the underlying reasons for the disagreement between the Diévert et al. [15] model and the data, we conduct simulations with an additional model constructed using RMG (see Section 3.2). As can be seen in Fig. 5a, the agreement between the RMG model (dashed lines) and the experimental data is similar to the Diévert et al. [15] model for the $P_C = 15$ bar, $\phi = 0.25$ and 0.5 data. Moreover, the RMG model predicts a similar NTC region as temperature

314 is decreasing. For the $P_C = 15$ bar, $\phi = 2.0$ data, the RMG model tends to
 315 over-predict the low-temperature overall ignition delays (i.e., those to the right
 316 of the experimental NTC region on the Arrhenius plot), and does not predict the
 317 NTC region found experimentally. As before, the trend at $P_C = 30$ bar, $\phi = 1.0$
 318 is similar to the $P_C = 15$ bar, $\phi = 2.0$ data; the RMG model over-predicts the
 319 low-temperature overall ignition delays and does not predict the experimental
 320 NTC region. Finally, as in the Diévar et al. [15] model, two-stage ignition is
 321 predicted for all of the $\phi = 1.0$ and $\phi = 2.0$ data shown in Fig. 5. However,
 322 the first-stage ignition delays are 0.1 ms to 0.5 ms less than the overall ignition
 323 delays, and are not shown on Fig. 5 because they are nearly indistinguishable
 324 from the overall ignition delay.

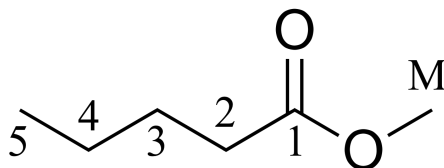
325 It is clear that neither model is able to predict the ignition delays of MV
 326 particularly well. In addition to the poor agreement shown in Fig. 5, the simu-
 327 lations for $P_C = 15$ bar, $\phi = 1.0$ and $P_C = 30$ bar, $\phi = 0.25, 0.5$ and 2.0 showed
 328 substantial heat release during the compression stroke (i.e., the simulations are
 329 much too reactive), and so these conditions are not compared in Fig. 5. We note
 330 again that the model by Diévar et al. [15] was validated for MV combustion
 331 only by comparison to flame extinction limits, so the disagreement is not wholly
 332 surprising.

333 In general, there could be three likely sources of error in the models: missing
 334 reaction pathways, incorrect values of the reaction rates, and incorrect values
 335 for thermodynamic properties of the species. We have noted in Section 3.2 that
 336 the RMG model has many more reactions than the Diévar et al. [15] model
 337 and the algorithm used in RMG considers a substantial number of the possible
 338 pathways. This reduces the possibility of missing reaction pathways affecting
 339 the model. Further detailed studies are required to ensure that the RMG model
 340 includes all of the relevant reaction pathways, which are outside the scope of
 341 this work.

342 The second source of error may be incorrect reaction rate parameters, either
 343 because the rates are specified incorrectly in the model or because the rates are
 344 not well estimated by the typical analogy based-rules. It should be noted that

errors of this type may affect the model generated by RMG—if the rates are not estimated correctly, reactions that are important in reality may not be included in the model. Determining the accuracy of the reaction rates used in the RMG and Diévert et al. [15] models requires further detailed studies of the models, which are also outside the scope of this work. Another, related, source of error could be incorrect estimation of the pressure dependence of the reaction rates, which may be particularly important for the isomerization reactions prevalent in low-temperature chemistry.

The third source of error may lie in the estimation of the thermodynamic properties of the species, particularly the fuel radicals. In the work of Diévert et al. [15], the program THERM [43] was used to estimate thermodynamic values using the group additivity method. In the RMG model constructed in this work, RMG itself estimates the thermodynamic properties of the molecules also using the group additivity method. Nonetheless, the two models have differing predictions of the thermodynamic properties of the species in the model, particularly the fuel and its radicals. The values of the heats of formation of the fuel and its H-atom abstraction radicals are shown in Table 3; the radicals are labeled according to the convention shown in Fig. 7.



363

Figure 7: Structure of MV with carbon atoms labeled according to the convention used in Table 3 and Table 4

364

Table 3: Heats of formation of MV and its radicals, labeled according to the convention used in Fig. 7

365

Radical Site	Diévar et al. [15]		RMG Model (this work)	
	[kJ/mol]	[kcal/mol]	[kJ/mol]	[kcal/mol]
MV	-470.98	-112.57	-472.53	-112.94
2	-297.16	-71.02	-273.63	-65.40
3	-277.03	-66.21	-273.63	-65.40
4	-277.03	-66.21	-278.61	-66.59
5	-265.94	-63.56	-267.53	-63.94
M	-270.51	-64.65	-270.12	-64.56

Table 3 shows that the heats of formation of the fuel and radicals 3, 4, 5, and M are quite similar between the two mechanisms. However, the heat of formation of the second radical, the one closest to the methyl ester group, has a significantly lower heat of formation in the model by Diévar et al. [15] than in the RMG model. Note that it is expected that the second radical will be somewhat more stable than the other radicals, due to the influence of the methyl ester group on the adjacent carbon atom.

This difference in heats of formation affects the pathways that consume the fuel. By conducting a reaction pathway analysis to determine which radicals are formed from the breakdown of the fuel, we can analyze the proportion of each radical formed as the fuel breaks down during the autoignition process. The following analysis is conducted for a constant volume, adiabatic simulation with initial temperature and pressure of 700 K and 30 bar, respectively, and for the stoichiometric equivalence ratio. The rates of production of the species have been integrated until the time of 20 % fuel consumption. The results of this analysis are shown in Table 4 for the two models. The percentages shown in Table 4 are the percent of the fuel consumed to form a particular fuel radical by all the reactions that can form that radical, and the radicals are labeled according to the convention in Fig. 7.

Table 4: Percent of MV consumed to form fuel radical species with a hydrogen atom missing at the location indicated in the first column and Fig. 7

387

	Radical Site	Diévert et al. [15] [%]	RMG Model [%]	RMG switched [%]
	2	29.2	12.5	11.0
388	3	17.5	12.2	11.1
	4	17.5	50.6	56.6
	5	9.5	3.9	4.3
	M	26.3	20.8	16.9

389 At the relatively low temperature and high pressure condition of this analy-
390 sis, all of the fuel is consumed by H-atom abstractions to form the fuel radicals
391 shown. It can be seen that the two models have quite different distributions
392 of products from the first H-abstraction reactions. The model of Diévert et al.
393 [15] predicts that H-abstraction from the second carbon is the most prevalent,
394 while the RMG model predicts that the radical on the fourth carbon in the
395 chain will be primarily formed. This is in line with the heats of formation in
396 Table 3, where the most stable radical (i.e., the radical with the smallest heat
397 of formation) is most likely to be formed in each model.

398 To further compare the models with each other, the NASA polynomials
399 representing the thermodynamic properties of MV and the 5 fuel radicals from
400 the model of Diévert et al. [15] are used to replace the equivalent molecules
401 in the RMG model. The results of a path analysis at the same condition as
402 the other analysis is shown in Table 4 in the “RMG switched” column. The
403 results of the analysis of the “RMG switched” model show that the radical on
404 the fourth carbon is still the most prevalent, despite the heats of formation for
405 the fuel radicals in the “RMG switched” model being identical to the Diévert
406 et al. [15] model. This suggests that the reaction pathways have a substantial
407 impact on the simulation, in addition to the influence of the thermochemistry,
408 as discussed previously. Moreover, since the thermochemistry of the species in
409 a reaction controls the reverse reaction rate of a reaction, the RMG algorithm
410 may miss important pathways due to improperly estimated thermochemistry.

411 Taken together, these results show that the poor performance in a given

412 model cannot be attributed to a single source. Separating the influence of ther-
413 mochemistry and kinetics requires further detailed study of the methyl valerate
414 system specifically, and methyl ester systems more generally. Although such
415 detailed work has begun, for example, with the work of Hayes and Burgess
416 [14], further work is required to accurately predict the low temperature ignition
417 delays of methyl valerate.

418 6. Conclusions

419 In this study, we have measured ignition delays for methyl valerate over a
420 wide range of engine-relevant pressures, temperatures, and equivalence ratios.
421 An NTC region of the overall ignition delay and two-stage ignition are recorded
422 for pressures of 15 bar at $\phi = 2.0$ and 30 bar at $\phi = 1.0$. A detailed chemical
423 kinetic model available in the literature is unable to reproduce the experimental
424 results, so a new model is constructed using the Reaction Mechanism Generator
425 software. Although the new model contains many more reactions than the
426 literature model, it is still unable to predict the experimental ignition delays
427 satisfactorily. Both models predict an NTC region of the overall ignition delay
428 under conditions where none is found in the experiments, and fail to predict
429 the NTC region of overall ignition delay that is present in the experiments.
430 Possible reasons for the discrepancy include missing reaction pathways, incorrect
431 rate estimates, and incorrect thermodynamic property estimates. Comparative
432 analysis of the two models failed to identify a single source of the error, and
433 further detailed studies are required to improve predictions of the ignition delay
434 at these engine-relevant conditions.

435 7. Acknowledgments

436 The authors acknowledge support from the Combustion Energy Frontier
437 Research Center, an Energy Frontier Research Center funded by the U.S. De-
438 partment of Energy, Office of Science, Office of Basic Energy Sciences, under
439 award number DE-SC0001198.

References

- [1] S. K. Hoekman, C. Robbins. Review of the effects of biodiesel on NO_x emissions. *Fuel Processing Technology* 96 (2012) 237–249. doi:10.1016/j.fuproc.2011.12.036.
- [2] J. Y. Lai, K. C. Lin, A. Violi. Biodiesel combustion: Advances in chemical kinetic modeling. *Progress in Energy and Combustion Science* 37 (2011) 1–14. doi:10.1016/j.pecs.2010.03.001.
- [3] L. Coniglio, H. Bennadji, P. Glaude, O. Herbinet, F. Billaud. Combustion chemical kinetics of biodiesel and related compounds (methyl and ethyl esters): Experiments and modeling – Advances and future refinements. *Progress in Energy and Combustion Science* 39 (2013) 340–382. doi:10.1016/j.pecs.2013.03.002.
- [4] W. K. Metcalfe, S. Dooley, H. J. Curran, J. M. Simmie, A. M. El-Nahas, M. V. Navarro. Experimental and modeling study of C₅H₁₀O₂ ethyl and methyl esters. *The Journal of Physical Chemistry A* 111 (2007) 4001–4014. doi:10.1021/jp067582c.
- [5] S. M. Walton, M. S. Wooldridge, C. K. Westbrook. An experimental investigation of structural effects on the auto-ignition properties of two C₅ esters. *Proceedings of the Combustion Institute* 32 (2009) 255–262. doi:10.1016/j.proci.2008.06.208.
- [6] S. Dooley, H. J. Curran, J. M. Simmie. Autoignition measurements and a validated kinetic model for the biodiesel surrogate, methyl butanoate. *Combustion and Flame* 153 (2008) 2–32. doi:10.1016/j.combustflame.2008.01.005.
- [7] B. Akih-Kumgeh, J. M. Bergthorson. Comparative Study of Methyl Butanoate and n -Heptane High Temperature Autoignition. *Energy & Fuels* 24 (2010) 2439–2448. doi:10.1021/ef901489k.

- 467 [8] B. Akih-Kumgeh, J. M. Bergthorson. Structure-reactivity trends of C1–C4
468 alkanoic acid methyl esters. *Combustion and Flame* 158 (2011) 1037–1048.
469 doi:10.1016/j.combustflame.2010.10.021.
- 470 [9] K. Hadj-Ali, M. Crochet, G. Vanhove, M. Ribaucour, R. Minetti. A study
471 of the low temperature autoignition of methyl esters. *Proceedings of the*
472 *Combustion Institute* 32 (2009) 239–246. doi:10.1016/j.proci.2008.09.002.
- 473 [10] K. Kumar, C.-J. Sung. Autoignition of methyl butanoate under en-
474 gine relevant conditions. *Combustion and Flame* 171 (2016) 1–14.
475 doi:10.1016/j.combustflame.2016.04.011.
- 476 [11] E. Fisher, W. J. Pitz, H. J. Curran, C. K. Westbrook. Detailed chem-
477 ical kinetic mechanisms for combustion of oxygenated fuels. *Proceed-*
478 *ings of the Combustion Institute* 28 (2000) 1579–1586. doi:10.1016/S0082-
479 0784(00)80555-X.
- 480 [12] O. Korobeinichev, I. Gerasimov, D. Knyazkov, A. Shmakov, T. Bolshova,
481 N. Hansen, C. K. Westbrook, G. Dayma, B. Yang. An Experimental and
482 Kinetic Modeling Study of Premixed Laminar Flames of Methyl Pentanoate
483 and Methyl Hexanoate. *Zeitschrift für Physikalische Chemie* 229 (2015).
484 doi:10.1515/zpch-2014-0596.
- 485 [13] A. M. Dmitriev, D. A. Knyazkov, T. A. Bolshova, A. G. Shmakov,
486 O. P. Korobeinichev. The effect of methyl pentanoate addition on
487 the structure of premixed fuel-rich n-heptane/toluene flame at at-
488 mospheric pressure. *Combustion and Flame* 162 (2015) 1964–1975.
489 doi:10.1016/j.combustflame.2014.12.015.
- 490 [14] C. Hayes, D. R. Burgess. Exploring the oxidative decompositions of methyl
491 esters: Methyl butanoate and methyl pentanoate as model compounds for
492 biodiesel. *Proceedings of the Combustion Institute* 32 (2009) 263–270.
493 doi:10.1016/j.proci.2008.05.075.

- [15] P. Diévar, S. H. Won, J. Gong, S. Dooley, Y. Ju. A comparative study of the chemical kinetic characteristics of small methyl esters in diffusion flame extinction. *Proceedings of the Combustion Institute* 34 (2013) 821–829. doi:10.1016/j.proci.2012.06.180.
- [16] G. Mittal, C.-J. Sung. A Rapid Compression Machine for Chemical Kinetics Studies at Elevated Pressures and Temperatures. *Combustion Science and Technology* 179 (2007) 497–530. doi:10.1080/00102200600671898.
- [17] G. Mittal, C.-J. Sung. Aerodynamics inside a rapid compression machine. *Combustion and Flame* 145 (2006) 160–180. doi:10.1016/j.combustflame.2005.10.019.
- [18] B. W. Weber, C.-J. Sung. UConnRCMPy: Python-based Data Analysis for Rapid Compression Machines. in: S. Benthall, S. Rostrup (Eds.), *Proceedings of the 15th Python in Science Conference*, pp. 36–44. http://conference.scipy.org/proceedings/scipy2016/bryan_weber.html.
- [19] B. W. Weber, R. Fang, C.-J. Sung. UConnRCMPy, 2017. v3.0.5. doi:10.5281/zenodo.815569.
- [20] D. G. Goodwin, H. K. Moffat, R. L. Speth. *Cantera: An Object-oriented Software Toolkit for Chemical Kinetics, Thermodynamics, and Transport Processes*, 2017. v2.3.0. doi:10.5281/zenodo.170284.
- [21] S. van der Walt, S. C. Colbert, G. Varoquaux. The NumPy Array: A Structure for Efficient Numerical Computation. *Computing in Science & Engineering* 13 (2011) 22–30. doi:10.1109/MCSE.2011.37.
- [22] E. Jones, T. Oliphant, P. Peterson, et al. *SciPy: Open source scientific tools for Python*, 2001–. <https://scipy.org>.
- [23] J. D. Hunter. Matplotlib: A 2D Graphics Environment. *Computing in Science & Engineering* 9 (2007) 90–95. doi:10.1109/MCSE.2007.55.

- [24] D. Lee, S. Hochgreb. Rapid Compression Machines: Heat Transfer and Suppression of Corner Vortex. *Combustion and Flame* 114 (1998) 531–545. doi:10.1016/S0010-2180(97)00327-1.
- [25] B. W. Weber, K. Kumar, Y. Zhang, C.-J. Sung. Autoignition of n-butanol at elevated pressure and low-to-intermediate temperature 158 (???) 809–819. doi:10.1016/j.combustflame.2011.02.005.
- [26] K. Kumar, G. Mittal, C.-J. Sung. Autoignition of n-decane under elevated pressure and low-to-intermediate temperature conditions 156 (???) 1278–1288. doi:10.1016/j.combustflame.2009.01.009.
- [27] A. K. Das, C.-J. Sung, Y. Zhang, G. Mittal. Ignition delay study of moist hydrogen/oxidizer mixtures using a rapid compression machine 37 (???) 6901–6911. doi:10.1016/j.ijhydene.2012.01.111.
- [28] J. Ortega, F. Espiau, J. Tojo, J. Canosa, A. Rodríguez. Isobaric Vapor-Liquid Equilibria and Excess Properties for the Binary Systems of Methyl Esters + Heptane. *Journal of Chemical & Engineering Data* 48 (2003) 1183–1190. doi:10.1021/je030117d.
- [29] A. G. Camacho, J. M. Moll, S. Canzonieri, M. A. Postigo. Vapor-Liquid Equilibrium Data for the Binary Methyl Esters (Butyrate, Pentanoate, and Hexanoate) (1) + Propanenitrile (2) Systems at 93.32 kPa. *Journal of Chemical & Engineering Data* 52 (2007) 871–875. doi:10.1021/je060469v.
- [30] R. M. Stephenson, S. Malanowski, D. Ambrose, *Handbook of the Thermodynamics of Organic Compounds*, Elsevier, New York, 1987.
- [31] A. C. van Genderen, J. van Miltenburg, J. G. Blok, M. J. van Bommel, P. J. van Ekeren, G. J. van den Berg, H. A. Oonk. Liquid–vapour equilibria of the methyl esters of alkanolic acids: Vapour pressures as a function of temperature and standard thermodynamic function changes. *Fluid Phase Equilibria* 202 (2002) 109–120. doi:10.1016/S0378-3812(02)00097-3.

- [32] S. P. Verevkin, V. N. Emel'yanenko. Transpiration method: Vapor pressures and enthalpies of vaporization of some low-boiling esters. *Fluid Phase Equilibria* 266 (2008) 64–75. doi:10.1016/j.fluid.2008.02.001.
- [33] E. E. Dames, A. S. Rosen, B. W. Weber, C. W. Gao, C.-J. Sung, W. H. Green. A detailed combined experimental and theoretical study on dimethyl ether/propane blended oxidation. *Combustion and Flame* 168 (2016) 310–330. doi:10.1016/j.combustflame.2016.02.021.
- [34] A. C. Hindmarsh, P. N. Brown, K. E. Grant, S. L. Lee, R. Serban, D. E. Shumaker, C. S. Woodward. SUNDIALS: Suite of nonlinear and differential/algebraic equation solvers. *ACM Transactions on Mathematical Software* 31 (2005) 363–396. doi:10.1145/1089014.1089020.
- [35] S. C. Chapra, R. P. Canale, *Numerical Methods for Engineers*, McGraw-Hill Higher Education, Boston, 6th ed edition, 2010.
- [36] B. W. Weber, K. E. Niemeyer. ChemKED: A human- and machine-readable data standard for chemical kinetics experiments. Submitted to: *International Journal of Chemical Kinetics* (2017). [arXiv:1706.01987](https://arxiv.org/abs/1706.01987).
- [37] J. W. Allen, C. F. Goldsmith, W. H. Green. Automatic estimation of pressure-dependent rate coefficients. *Physical Chemistry Chemical Physics* 14 (2012) 1131–1155. doi:10.1039/c1cp22765c.
- [38] B. W. Weber, C.-J. Sung, M. W. Renfro. On the uncertainty of temperature estimation in a rapid compression machine. *Combustion and Flame* 162 (2015) 2518–2528. doi:10.1016/j.combustflame.2015.03.001.
- [39] G. Kukkadapu, K. Kumar, C.-J. Sung, M. Mehl, W. J. Pitz. Experimental and surrogate modeling study of gasoline ignition in a rapid compression machine. *Combustion and Flame* 159 (2012) 3066–3078. doi:10.1016/j.combustflame.2012.05.008.
- [40] M. Ribaucour, R. Minetti, L. R. Sochet. Autoignition of n-pentane and 1-pentene: Experimental data and kinetic modeling. *Symposium*

- 575 (International) on Combustion 27 (1998) 345–351. doi:10.1016/S0082-
576 0784(98)80422-0.
- 577 [41] J. Bugler, K. P. Somers, E. J. Silke, H. J. Curran. Revisiting the Ki-
578 netics and Thermodynamics of the Low-Temperature Oxidation Pathways
579 of Alkanes: A Case Study of the Three Pentane Isomers. The Journal of
580 Physical Chemistry A 119 (2015) 7510–7527. doi:10.1021/acs.jpca.5b00837.
- 581 [42] K. A. Heufer, J. Bugler, H. J. Curran. A comparison of longer alkane
582 and alcohol ignition including new experimental results for n-pentanol and
583 n-hexanol. Proceedings of the Combustion Institute 34 (2013) 511–518.
584 doi:10.1016/j.proci.2012.05.103.
- 585 [43] E. R. Ritter, J. W. Bozzelli. THERM: Thermodynamic property estimation
586 for gas phase radicals and molecules. International Journal of Chemical
587 Kinetics 23 (1991) 767–778. doi:10.1002/kin.550230903.